ELSEVIER

Journal of Nuclear Materials 283–287 (2000) 1028–1032

journal of nuclear materials

www.elsevier.nl/locate/jnucmat

Damage mechanisms and fracture toughness of GlidCop® CuAl25 IG0 copper alloy

S. Tähtinen [a,*], A. Laukkanen [a], B.N. Singh [b]

[a] *VTT Manufacturing Technology, P.O. Box 1704, FIN-02044 VTT, Finland*
[b] *Materials Research Department, Risø National Laboratory, DK-4000 Roskilde, Denmark*

Abstract

Crack nucleation and growth behaviour are important parameters in deciding about the applicability of the dispersion strengthened copper alloy CuAl25 in components such as the first wall and divertor in ITER. The effective strain to fracture of notched tensile specimens decreased with increasing stress state triaxiality and with increasing temperature at constant constraint level following the Rice and Tracey model for void growth. In three point bend tests, the strain for stable crack initiation decreased significantly with increasing temperature. The CuAl25 alloy failed by a ductile microvoid mechanism where extensive void nucleation occurred at very low strains at grain boundaries with increasing stress state triaxiality. At elevated temperatures the fracture surface morphology changed from microvoid to intergranular fracture in three-point bend tests.

1. Introduction

Dispersion strengthened copper alloys are of technological interest due to their high thermal and electrical conductivity combined with a relatively high mechanical strength. These alloys have been shown to be thermally stable and resist recrystallisation during thermal annealing at temperatures approaching the melting temperature of copper. The current design for ITER utilizes copper alloys in the first wall and divertor components and the anticipated operating temperature for copper alloys is in the range of 100–350°C.

On the basis of the currently available data, the dispersion strengthened CuAl25 alloy is being considered as the primary candidate alloy for ITER first wall components. Recent experimental results indicate that the loss of strain hardening capacity, the loss of uniform elongation, the marked reduction in fracture toughness and the strain rate sensitivity are serious deficiencies in the performance of the CuAl25 alloy at elevated temperatures under neutron irradiation [1–6]. The experimental results on notched tensile and three-point bend specimens are presented and the fracture mechanisms are discussed in the present paper.

2. Experimental details

The copper alloy GlidCop® CuAl25 IG0 (ITER Grade 0) produced by OMG Americas was studied. The details of the microstructure of CuAl25 IG0 alloy is presented in [1,7–9]. Smooth and circumferentially notched round tensile specimens with varying notch root radius were tested at room temperature (22°C) and 150°C to establish the stress-state dependency of the fracture strain. The initial notch root radii 0.5, 2 and 4 mm were applied at a constant initial notch root diameter of 6 mm with the nominal outer diameter of 10 mm. The applied strain rate was 2×10^{-4} s^{-1} and both the axial extension and the diametric contraction were measured with strain gages. The initial stress state triaxiality (σ_m/σ_{fl}) in the central region of the specimen and the effective plastic strain at fracture (ϵ_f) were estimated based on the Bridgman analysis [10] as a ratio of the mean stress (σ_m) to the flow stress (σ_{fl}) and as a ratio of diametric contraction, where d_i is the initial and d_f the

* Corresponding author. Tel.: +358-9 456 6859; fax: +358-9 456 7002.
E-mail address: seppo.tahtinen@vtt.fi (S. Tähtinen).

0022-3115/00/$ - see front matter
PII: S0022-3115(00)00201-4

final notch root diameter and r is the notch root radius, respectively, by

$$\sigma_m/\sigma_{fl} = 1/3 + \ln(d_i/4r + 1), \quad (1)$$

$$\epsilon_f = 2\ln(d_i/d_f). \quad (2)$$

Single edge bend SE(B) fracture toughness specimens of dimensions $3 \times 4 \times 27$ mm^3 were machined from plates of the above described copper alloy and were tested both in the unirradiated and neutron irradiated conditions. The notch with a radius of 0.15 mm and the 20% side grooves were machined by applying electric wire discharged machining. Specimens with a sharp prefatigued crack as well as specimens with a blunt notch had the same initial crack or notch length to specimen width ratio of about $a_0/W = 0.5$. Fracture resistance curves were determined using a displacement-controlled three-point bend test with a constant displacement rate of 1.5×10^{-2} mm min^{-1}. Fracture resistance tests at elevated temperatures were carried out in a silicon oil bath. Load, displacement and crack length were measured using the direct current potential drop (DC-PD) method and were recorded during testing. The fracture resistance curves were determined following the ASTM 1737 standard procedure.

3. Results

3.1. Notched tensile tests

The effective plastic strain to fracture as a function of the stress state triaxiality or constraint ratio for CuAl25 IG0 at 22°C and 150°C is presented in Fig. 1. The effective plastic strain to fracture decreased significantly with increasing constraint ratio, and at constant constraint ratio it decreased with increasing temperature. As a first approximation, the fracture strain dependence with stress state triaxiality were fitted to a theoretical estimate based on Rice and Tracey's equation developed for void growth [11] in the form

$$\epsilon_f = \alpha \exp(-\beta\sigma_m/\sigma_{fl}). \quad (3)$$

The least-squares curve fit was employed to determine the parameters α and β at both test temperatures, giving values of 1.6–1.7 and 1.1–1.6, respectively. The theoretical value for the stress state sensitivity parameter β according to Rice and Tracey's model is 1.5, which is reasonably close to the obtained values of 1.1 and 1.6.

The macroscopic fracture surface appearance changed with increasing constraint ratio and testing temperature. The fraction of high constraint area in the middle of the specimen cross-section with stable crack growth increased in proportion to the shear area with increasing triaxial stress state and increasing test temperature. Also the overall roughness within the high constraint area seemed to increase with increasing constraint ratio especially at the ambient temperature. The microscopic fracture surface morphology showed a ductile microvoid type of fracture. The dimple size and distribution were independent of initial constraint level and only a modest decrease in dimple size from 4–5 to 2–3 μm was observed with increasing temperature.

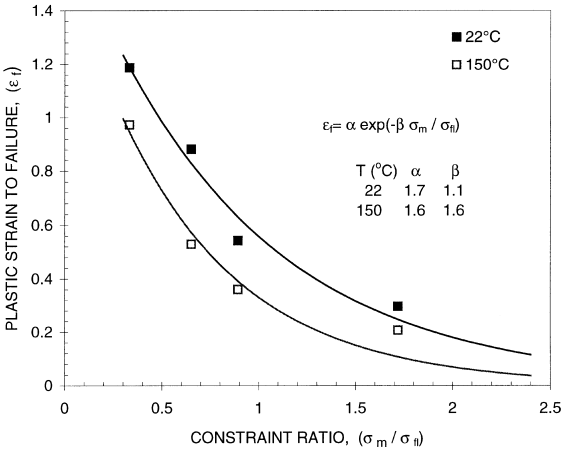

Fig. 1. The stress state dependent effective plastic strain to failure for CuAl25 IG0 alloy at 22°C and 150°C together with numerical fitting of Rice and Tracey's void growth models. The effective plastic strain to failure at constant constraint ratio is lower at elevated temperatures compared to that at the ambient temperature.

3.2. Notched three-point bend tests

Fig. 2 illustrates the normalised load and load-line displacement curves for the CuAl25 IG0 alloy and the corresponding normalised potential drop curves at different test temperatures. The crack initiation can be identified as a point where the potential drop values deviate from the linear dependence on the load-line displacement. The load and displacement values required to initiate stable crack growth were significantly higher in specimens with a blunt notch compared to specimens with a sharp fatigue crack at both test temperatures. The extent of plastic deformation – e.g. blunting of the crack tip area in specimens with a blunt notch – is clearly illustrated with the linear increase of potential drop value with increasing load-line displacement.

The fracture surface morphologies of SE(B) fracture toughness specimens with a sharp fatigue crack and a blunt notch were basically similar; well-defined stretch zones prior to stable crack propagation were observed in both cases on the fracture surfaces at ambient temperature. The stretch zone width increased two-fold from 40 to 80 μm when the sharp fatigue crack was replaced with

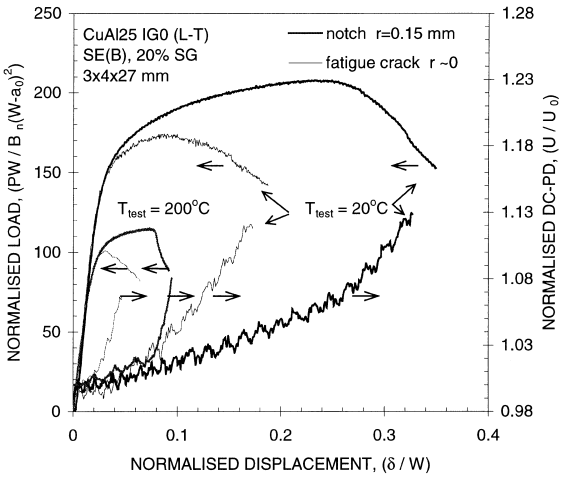

Fig. 2. Normalised load and potential drop signals versus load-line displacement of three-point bend specimens of CuAl25 IG0 alloy tested at: 20°C and 200°C with sharp fatigue crack and blunt notch with notch root radius of 0.15 mm. Note that higher amount of plastic straining e.g. crack tip blunting (linear increase in DC-PD potential signal) and higher strength level are required for crack initiation in specimens with blunt notch (low constraint) compared to sharp crack (high constraint).

a blunt notch with the notch root radius of 0.15 mm. At elevated temperatures the stable crack propagation seemed to start immediately from the sharp fatigue crack tip without any clear indication of a stretch zone. The fracture surface morphology in the stable crack growth area at the ambient temperature was a typical ductile microvoid type of fracture which changed to intergranular fracture at the elevated temperature as illustrated in Fig. 3. The fracture surface morphology during the stable crack propagation was similar in specimens with a sharp fatigue crack and a blunt notch.

A damage mechanics analysis was performed in order to evaluate the critical process zone length or the characteristic distance related to different three-point bend specimen configurations and to determine the correspondence between micromechanics of failure and the predictions of damage mechanics models. This was carried out by determining the stress and strain fields ahead of the crack or notch tip using finite element methods and the modified Gurson model [14]. The attained hydrostatic stress and equivalent plastic strain fields were combined with the Rice and Tracey description of critical failure strain as a function of stress triaxiality, as indicated in Fig. 4, for specimens with a sharp fatigue crack. The process zone length was 3 and 175 μm for specimens with a sharp fatique crack and a blunt notch, respectively. It was found that the strain and stress gradients ahead of a sharp fatigue crack were orders of magnitude higher compared to the gradients ahead of the blunt notch.

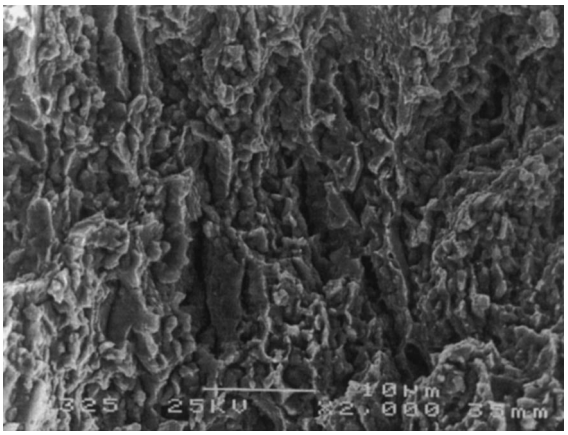

Fig. 3. SEM micrograph of fracture surface morphology of notched three-point bend specimen of CuAl25 IG0 alloy with the notch root radius of 0.15 mm tested at 200°C with constant load-line displacement rate of 0.015 mm min^{-1} showing low ductility grain boundary fracture mode.

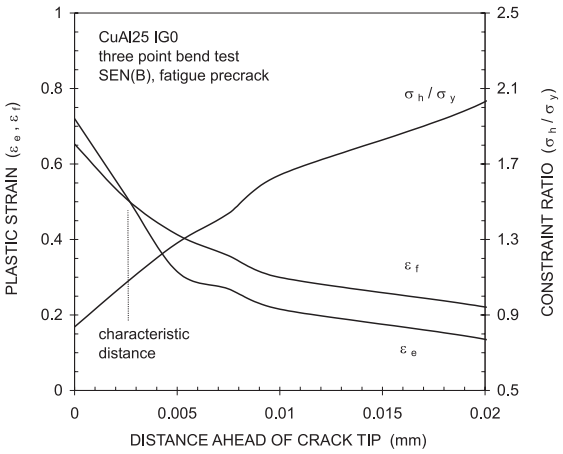

Fig. 4. The calculated equivalent plastic strain and level of triaxial stress state ahead of a sharp fatigue crack (nominal crack tip radius 10 μm) using modified Gurson model [14] together with critical plastic strain to fracture measured, with notch tensile specimens at room temperature. For fracture initiation, the equivalent plastic strain must exceed critical plastic strain to fracture within the process zone.

4. Discussion

The effective plastic strain to fracture decreased exponentially with increasing stress state triaxiality showing a relatively good correlation with Rice and Tracey's void growth model [11]. The effect of stress state triaxiality on ductile fracture, as has been observed in numerous experiments [10,12,13] and presented by the continuum models (e.g. modified Gurson [14] and Rice–Tracey [11]) indicates that the relative void growth rate

increases nearly exponentially with stress state triaxiality. However, the fracture surface morphology of CuAl25 IG0 alloy showed that dimple size, spacing and density were practically independent of constraint ratio and temperature. Only a minor decrease in dimple size and spacing was observed with increasing temperature. The observed microvoid structure cannot be explained exclusively by changes in void growth rate because the rate of void growth is obviously extremely limited due to very high density of void nuclei and subsequent coalescence even at low stress state triaxiality. It is suggested that as the constraint affects the stress and strain levels the resulting void nucleation occurs at very low strain values at high stress state triaxiality. Also the three-point bend tests showed initiation of stable crack propagation at very low displacement values in specimens with a sharp fatigue crack and blunt notch.

Despite the strain gradient in the notched specimen, which was an order of magnitude smaller than that in the precracked specimen, crack initiation was observed in both types of specimens and the resulting fracture surface morphologies were practically identical except for the larger blunting region in the notched specimen. On the basis of micromechanisms of fracture as described above, this can be correlated to the relative notch sensitivity of the CuAl25 IG0 alloy. The process zone length or the characteristic distance for the cracked specimen was about 3 μm, as illustrated in Fig. 4, and that for the notched specimen was about 175 μm. The fracture process zone size is a measure of the severity of the near crack tip stress and strain gradients. As the process zone length (or the characteristic distance) for cracked specimens was of the order of the grain size it is suggested that the ability for the crack to seek locally weak parts of the microstructure is enhanced and may result in a decrease in overall macroscopic fracture toughness. This is consistent with the observed change in the fracture mode from ductile dimple type to intergranular with a corresponding decrease in the fracture toughness at elevated temperatures [5,6].

It is of interest to point out here that the effect of test temperature on the fracture mode reported in the present work is very similar to the effect observed recently in low cycle fatigue experiments on the CuAl25 GlidCop alloy both in the unirradiated and irradiated conditions at test temperatures of 22 and 100°C. At both temperatures, the final failures were found to be ductile in nature and were dominated by large populations of plasticity-induced voids associated with alumina particles [15,16]. At test temperatures of 250 and 350°C, on the other hand, the fracture mode was found to be clearly brittle in nature, both in the unirradiated and irradiated CuAl25 GlidCop alloy [17].

The tensile ductility and plane strain fracture initiation toughness are commonly related to second phase particles and their size, distribution and volume fraction [18]. Two types of alumina particles have been reported in CuAl25 IG0 alloy; a low density of large (~0.1 μm) particles preferentially located at grain or subgrain boundaries and a high density of small about 7–12 nm particles non-homogeneously distributed within grains [1,7–9]. It is suggested that the combination of the large volume fraction of grain boundaries and the presence of alumina particles on these boundaries play a major role in erasing the observed loss of tensile ductility and fracture toughness properties. This is also supported by the estimated process zone size, which correlates well with the grain size of the alloy.

5. Conclusions

The effective plastic strain to fracture of the CuAl25 IG0 alloy was found to be strongly dependent on the stress state triaxiality, and those results were in good accord with the Rice and Tracey model. At a constant triaxial stress state level the effective plastic strain to fracture decreased with increasing temperature. The fracture mode was found to be ductile microvoid fracture where void nucleation and coalescence were enhanced and void growth was restricted with increasing stress state triaxiality. In precracked three point bend specimens the fracture surface morphology changed from ductile dimple at the ambient temperature to intergranular fracture at the elevated temperature. It is suggested that the large volume fraction of grain boundaries and the presence of alumina particles on these boundaries dominate the ductile fracture behaviour of CuAl25 IG0 alloy.

Acknowledgements

This work was performed under the frame work of European Fusion Technology Programme by Associations Euratom–Tekes and Euratom–Risø.

References

[1] B.N. Singh, D.J. Edwards, P. Toft, J. Nucl. Mater. 238 (1996) 244.
[2] B.N. Singh, D.J. Edwards, M. Eldrup, P. Toft, Risø Report, Risø-R-937 (EN), January 1997.
[3] B.N. Singh, D.J. Edwards, M. Eldrup, P. Toft, Risø Report, Risø-R-971 (EN), February 1997.
[4] S.A. Fabritsiev, S.J. Zinkle, B.N. Singh, J. Nucl. Mater. 233–237 (1996) 127.
[5] S. Tähtinen, M. Pyykkönen, P. Karjalainen-Roikonen, B.N. Singh, P. Toft, J. Nucl. Mater. 258–263 (1998) 1010.
[6] S. Tähtinen, M. Pyykkönen, B.N. Singh, P. Toft, in: M.L. Hamilton, A.S. Kumar, S.T. Rosiski, M.L. Grossbeck (Eds.), Effects of Radiation and Materials, The 19th

International Symposium, ASTM-STP 1366, Amer. Soc. Test. Mater., West Conshocker, PA, 2000, p. 1241.
[7] S.J. Zinkle, A. Horsewell, B.N. Singh, W.F. Sommer, J. Nucl. Mater. 195 (1992) 11.
[8] K.R. Anderson, F.A. Garner, M.L. Hamilton, J.F. Stubbins, in: R.E. Stoller, A.S. Kumar, D.S. Gelles (Eds.), 15th International Symposium, ASTM STP 1125, Amer. Soc. Test. Mater., Philadelphia, 1992, p. 854.
[9] H. Burlet, L. Guetaz, P. Bucci, J.M. Gentzbittel, I. Chu, N. Scheer, Note Technique DEM 98/75, CEA-CEREM, December 1998.
[10] A.C. MacKenzie, J.W. Hancock, D.K. Brown, Eng. Fract. Mech. 9 (1977) 167.
[11] J.R. Rice, D.M. Tracey, J. Mech. Phys. Solids 17 (1969) 201.
[12] B. Marini, F. Mudry, A. Pineau, Eng. Fract. Mech. 22 (1985) 989.
[13] M.J. Haynes, B.P. Somerday, C.L. Lack, R.P. Gangloff, in: R.S. Piascik, R.P. Gangloff, A. Saxena (Eds.), ASTM-STP 1297, Amer. Soc. Test. Mater., 1977, p. 165.
[14] A.L. Gurson, J. Eng. Mater. Technol. (1977) 2.
[15] B.N. Singh, J.F. Stubbins, P. Toft, Risø Report, Risø-R-991 (EN), May 1997.
[16] B.N. Singh, J.F. Stubbins, P. Toft, J. Nucl. Mater. 275 (1999) 125.
[17] B.N. Singh, J.F. Stubbins, P. Toft, Risø Report, Risø-R-1128 (EN), Mar. 2000.
[18] W.M. Garrison Jr., N.R. Moody, J. Phys. Chem. Solids 48 (1987) 1035.